Single-crystal structure determination and infrared reflectivity study of the Li_2CaHfF_8 scheelite

2002 J. Phys.: Condens. Matter 14 5485

(http://iopscience.iop.org/0953-8984/14/22/303)

INSTITUTE OF PHYSICS PUBLISHING JOURNAL OF PHYSICS: CONDENSED MATTER

J. Phys.: Condens. Matter **14** (2002) 5485–5495 PII: S0953-8984(02)35560-7

Single-crystal structure determination and infrared reflectivity study of the Li_2CaHfF_8 scheelite

A P Ayala[1], C W A Paschoal[1], J-Y Gesland[2], J Ellena[3], E E Castellano[3] and R L Moreira[4]

[1] Departamento de Física, Universidade Federal do Ceará, CP 6030, 60455-760 Fortaleza CE, Brazil
[2] Université du Maine—Cristallogenese, 72025 Le Mans Cedex 09, France
[3] Instituto de Física de São Carlos—USP, CP 369, 13560-970, São Carlos SP, Brazil
[4] Departamento de Física, ICEx, Universidade Federal de Minas Gerais, CP 702, 30123-970, Belo Horizonte MG, Brazil

E-mail: ayala@fisica.ufc.br

Received 5 April 2002
Published 23 May 2002
Online at stacks.iop.org/JPhysCM/14/5485

Abstract

The room-temperature crystal structure of Li_2CaHfF_8 is determined using high-precision single-crystal x-ray diffraction measurements. It is found to be tetragonal, belonging to the space group $I\bar{4}$ with $Z = 2$. The cell parameters are $a = 5.1063(2)$ Å and $c = 10.5248(5)$ Å. Polarized infrared reflectivity measurements are performed in order to obtain the phonon spectrum. Angular dispersion curves of polar modes are calculated to identify the presence of oblique phonons.

1. Introduction

The development of cheap and efficient semiconductor diode lasers led to a renewed interest in the fabrication of diode-pumped solid-state lasers. Among several compounds, fluoride crystals doped with trivalent rare-earth ions show the richest variety of laser wavelengths. Compounds such as $LiYF_4$ with trivalent rare-earth activators offer new laser properties almost every year [1]. Fluoride scheelites are compounds of the form $LiMF_4$, where M is a trivalent ion. M sites should be occupied by rare-earth ions, but the most investigated member of this family is $LiYF_4$, whose crystalline structure is isomorphic to that of scheelite ($CaWO_4$) and belongs to the $I4_1/a$ (C^6_{4h}) space group with four molecules per unit cell [2–4].

Due to the good optical properties of fluoride scheelites, a new family of these compounds was introduced by Védrine *et al* [5], where the yttrium ions are replaced by both a bivalent element (M^{II} = Ca, Cd) and a tetravalent one (M^{IV} = Th, U, Ce, Tb, Zr, Hf), establishing a 1–1 order. Hence, a double molecule is necessary to describe this structure, i.e. $Li_2M^{II}M^{IV}F_8$. Some time later, Védrine *et al* [6] reported an x-ray investigation of the Li_2CaUF_8 crystal.

According to their results, Li_2CaUF_8 has a body-centred tetragonal structure belonging to space group $I\bar{4}m2$ (D^9_{2d}), with $Z = 2$. In this structure, the sublattice formed by Li, Ca and U cations is equivalent to that of $LiYF_4$, where Ca and U are placed in the Y sites in an ordered way. The most important difference is found in the fluorine distribution, where the number of sites is doubled, each one being half occupied.

Recently, Ayala *et al* [7] have studied single crystals of Li_2CaHfF_8 by powder x-ray diffraction and polarized Raman scattering. X-ray results confirmed the tetragonal body-centred structure of this compound, but the Raman spectra did not agree with those predicted from the analysis of the space group proposed by Védrine *et al* [6]. Thus, a careful group theory analysis showed that the most probable space group is $I\bar{4}$ (S^2_4). Furthermore, the comparison between the vibrational modes of Li_2CaHfF_8 and $LiLnF_4$ (*Ln*: lanthanides) is in good agreement with the correlation between the irreducible representations of both S_4 and C_{4h} point groups, once the $I\bar{4}$ space group is a subgroup of the scheelite group. Additional support for the choice of the $I\bar{4}$ space group was obtained through electrical conductivity measurements in Li_2CaHfF_8 [8]. If fluorine vacancies are present, the structure belonging to the $I\bar{4}m2$ space group allows fluorine diffusion in all directions. However, electrical conductivity measurements showed that Li_2CaHfF_8 is a highly anisotropic ionic conductor, where, at 700 K, the conductivity in the $\boldsymbol{ab}$-plane is four orders of magnitude higher than those parallel to the $\boldsymbol{c}$-axis. This fact was explained by considering that the conductivity is mainly due to lithium diffusion, since there are lithium chains parallel to the $\boldsymbol{ab}$-plane, while along the (001) direction these chains are broken by the heavy ions.

Despite the fact that there is abundant experimental evidence supporting the idea that Li_2CaHfF_8 belongs to the $I\bar{4}$ space group, no structural data are available confirming this hypothesis. Thus, the aim of this work is to accomplish a high-precision single-crystal x-ray diffraction study, which provides the Li_2CaHfF_8 crystalline structure. Furthermore, polarized infrared reflectivity spectra are recorded in single crystals. The observed infrared-active phonons agree with the group theory predictions based on the $I\bar{4}$ space group and allow us, in addition to Raman-active phonons previously reported, to determine the complete vibrational spectra of the Li_2CaHfF_8 crystal.

2. Experimental details

In spite of an incongruent melting, several cubic centimetre single crystals of Li_2CaHfF_8 have been pulled from stoichiometric melts using the Czochralski technique. A colourless crystal of dimensions 0.05 mm × 0.07 mm × 0.10 mm was used for data collection. All measurements were made on an Enraf–Nonius Kappa-CCD difractometer with graphite monochromated Mo Kα ($\lambda = 0.710\,73$ Å) radiation. Data were collected up to 60° in 2θ, with a redundancy of four. The final unit-cell parameters were based on all reflections. Data collections were made by using the COLLECT program [9]; integration and scaling of the reflections were performed with the HKL Denzo-Scalepack system of programs [10]. Absorption corrections were carried out using the multi-scan method [11].

The structure was solved using Patterson methods with SHELXS-97 [12]. The Patterson map showed all atoms except the Li atoms. They were found in successive difference Fourier maps. The model was refined by full-matrix least-squares procedures on F^2 using SHELXL-97 [13]. The program WINGX was used to analyse and prepare the data for publication [14]. Crystal data, data collection procedures, structure determination methods and refinement results are summarized in table 1.

Reflection infrared spectra were recorded with a BOMEM DA8 Fourier transformer spectrometer, in the range 30–4000 cm^{-1}. The spectral resolution was typically 4 cm^{-1}.

Table 1. Crystal data and structure refinement.

Empirical formula	Li_2CaHfF_8
Formula weight	384.45
Temperature	293(2) K
Wavelength	0.710 73 Å
Crystal system	Tetragonal
Space group	$I\bar{4}$
Unit-cell dimensions	$\boldsymbol{a} = 5.1063(2)$ Å
	$\boldsymbol{c} = 10.5248(5)$ Å
Volume	274.43(2) Å^3
Z	2
Density (calculated)	4.653 mg m^{-3}
Absorption coefficient	20.047 mm^{-1}
$F(000)$	328
Crystal size	$0.10 \times 0.07 \times 0.05$ mm^3
Theta range for data collection	3.87°–30.00°
Index ranges	$-7 \leqslant h \leqslant 7, -7 \leqslant k \leqslant 7, -14 \leqslant l \leqslant 14$
Reflections collected	2203
Independent reflections	401 (R(int) = 0.1217)
Completeness to θ = 30.00	100.0%
Absorption correction [11]	Semi-empirical from equivalents
Max. and min. transmission	0.4339 and 0.2391
Refinement method	Full-matrix least squares on F^2
Computing[a]	COLLECT [9], HKL Denzo and Scalepack [10], SHELXS-97 [12], SHELXL-97 [13]
Data/parameters	401/26
Goodness of fit on F^2	1.155
Final R indices ($I > 2\sigma(I)$)	$R1 = 0.0326$, w$R2 = 0.0717$
R indices (all data)	$R1 = 0.0397$, w$R2 = 0.0724$
Absolute structure parameter	−0.06(4)
Extinction coefficient	0.101(10)
Largest diff. peak and hole	1.607 and −3.666 e Å^{-3}

[a] Data collection, data processing, structure solution and structure refinement respectively.

For the mid-infrared region (above 400 cm^{-1}), the best choice of accessories was a Globar source, a coated KBr beamsplitter and a nitrogen-cooled HgCdTe detector. The far-infrared region was measured using a Globar or Mercurium arc lamp (below 200 cm^{-1}), a 6 mm coated-Mylar hypersplitter^{TM} and a helium-cooled Si bolometer.

3. Results

3.1. X-ray diffraction

In complete agreement with the space group proposed by Ayala *et al* [8], the refinement of our single-crystal x-ray results confirms that Li_2CaHfF_8 belongs to the $I\bar{4}$ space group with two molecules per unit cell. Its lattice parameters are $\boldsymbol{a} = 5.1063(2)$ Å and $\boldsymbol{c} = 10.5248(5)$ Å, with a volume of 274.43(2) Å^3. Atomic positions and anisotropic displacement parameters are given in table 2. According to this table, two non-equivalent lithiums occupy sites with tetrahedral coordination, with Li(1) and Li(2) surrounded by four F(1) (Li(1)–F(1) = 1.9044 Å) and F(2) (Li(2)–F(2) = 1.9018 Å) anions, respectively. Heavy cations, hafnium and calcium,

Table 2. Atomic coordinates ($\times 10^4$), equivalent isotropic displacement parameters (Å$^2 \times 10^3$) and anisotropic displacement parameters (Å$^2 \times 10^3$). $U(eq)$ is defined as one-third of the trace of the orthogonalized U_{ij} tensor. The anisotropic displacement factor exponent takes the form $-2\pi^2[h^2a^{*2}U_{11} + \cdots + 2hka^*b^*U_{12}]$.

	x	y	z	$U(eq)$	U_{11}	U_{22}	U_{33}	U_{23}	U_{13}	U_{12}
Li(1)	0	5000	2500	19(4)	16(6)	16(6)	25(11)	0	0	0
Li(2)	0	0	5000	19(4)	16(6)	16(6)	25(11)	0	0	0
Ca	5000	5000	5000	14(1)	15(1)	15(1)	12(2)	0	0	0
Hf	5000	0	2500	14(1)	14(1)	14(1)	13(1)	0	0	0
F(1)	2886(11)	6868(11)	3204(5)	17(1)	16(2)	16(2)	17(2)	1(2)	−3(2)	−5(2)
F(2)	2877(13)	1468(12)	4102(6)	19(1)	18(2)	19(3)	18(3)	−4(2)	6(2)	−3(2)

are located at the centre of a coordination polyhedron determined by four F(1) and four F(2). Due to the higher valence of the hafnium, fluorine ions are closer to this cation (Hf–F $\sim$ 2.10 Å) than to calcium (Ca–F $\sim$ 2.33 Å).

After obtaining the Li_2CaHfF_8 structure, it is possible to compare it with that of other fluoride scheelites, that is, the $I4_1/a$ (C_{4h}^6) space group with four molecules per unit cell and approximately the same lattice parameters [2, 3]. For example, in the $LiYF_4$ structure, cations occupy sites with the same coordination polyhedra, but all lithium and yttrium sites are equivalent. Replacing yttrium by hafnium and calcium in an ordered way, these sites split into two sets of non-equivalent sites. Due to this fact, the inversion centre is lost in the Li_2CaHfF_8 structure, which also produces the splitting of lithium and fluorine ions into two non-equivalent sets. Since a doubled molecule ($2Li(Hf,Ca)F_4$) is necessary to describe the new scheelite structure and the number of atoms per unit cell remains constant, the number of molecules per unit cell must be reduced by a factor of two.

3.2. Group theory predictions

A detailed factor group analysis of the possible space groups has been achieved by Ayala *et al* [7] in order to identify the most probable space group for the Li_2CaHfF_8 scheelite. Based on this analysis and polarized Raman scattering results, the $I\bar{4}$ (S_4^2) space group was proposed and confirmed in this work. Thus, the irreducible representation of normal optical modes at the Brillouin zone centre (Γ point) obtained using the method of site group analysis proposed by Rousseau *et al* [15] is

$$\Gamma_{vib} = 6\mathrm{A} + 9\mathrm{B} + 9\mathrm{E}. \tag{1}$$

All irreducible representations of the S_4 factor group are Raman active, while B and E are infrared active and should be observed by using polarized radiation parallel and perpendicular to the $\boldsymbol{c}$-axis, respectively.

3.3. Infrared reflectivity

The infrared dielectric function was determined by carrying out a dispersion analysis of the observed spectra on the basis of the four-parameter semi-quantum model [16]. According to this model, the complex dielectric constant is expressed in terms of the infrared active modes as follows:

$$\varepsilon(\omega) = \varepsilon_\infty \prod_j \frac{\omega_{jLO}^2 - \omega^2 + \mathrm{i}\omega\gamma_{jLO}}{\omega_{jTO}^2 - \omega^2 + \mathrm{i}\omega\gamma_{jTO}}, \tag{2}$$

Table 3. Dispersion parameters for the best fit to the reflectivity data of Li_2CaHfF_8 crystals at 300 K.

ω_{TO} (cm^{-1})	γ_{TO} (cm^{-1})	ω_{LO} (cm^{-1})	γ_{TO} (cm^{-1})	$\Delta\varepsilon$
$E\|z$		$\varepsilon_\infty^{\|} = 2.417$		
117	36	124	90	—
153	17	153	18	0.118
170	9	172	8	0.401
182	45	190	63	—
208	10	213	8	0.715
254	13	290	10	2.897
329	25	349	15	1.268
358	19	374	12	0.388
379	14	409	14	0.216
423	18	458	17	0.302
458	18	561	27	0.005
$E\perp z$		$\varepsilon_\infty^{\perp} = 2.288$		
119	4	134	6	1.718
185	6	198	7	0.751
212	9	214	7	0.063
293	17	307	12	0.630
344	16	362	8	0.542
363	6	364	22	0.002
400	15	405	16	0.173
424	24	445	41	0.540
465	60	578	49	0.441

where ω_{jTO} and ω_{jLO} correspond to the resonance frequencies of the jth transverse and longitudinal modes, respectively, and γ_{jTO} and γ_{jLO} are the corresponding damping factors. ε_∞ is the dielectric constant due to electronic polarizations. The observed infrared reflectivity $\boldsymbol{R}$ is fitted with the aid of equation (2), together with

$$\boldsymbol{R} = \left|\frac{\sqrt{\varepsilon}-1}{\sqrt{\varepsilon}+1}\right|^2. \tag{3}$$

The reflectivity spectra of Li_2CaHfF_8 are shown in figure 1, for polarization (a) parallel and (b) perpendicular to the c-axis. The spectra calculated by using the method outlined above [17] fitted very well to the experimental ones. Table 3 lists the parameters of longitudinal and transversal modes used to obtain the best fit to the reflectivity curves. As a result, we obtained 11 and nine bands in the spectra taken with the polarization parallel and perpendicular to the principal axis, respectively. Since the group theory analysis predicts nine infrared-active modes in each geometry, two bands in the first spectrum must be due to polarization leaks. These bands, indicated by arrows in figure 1, can be identified by comparing the top and bottom sections of table 3, where the first and fourth bands of the top section are highly damped and located close to the first and second bands of the bottom section, which are the most intense and well defined bands in the $\boldsymbol{E}\perp\boldsymbol{z}$ spectrum. Once the infrared-active vibrational modes are determined, the oscillator strength $\Delta\varepsilon_j$ of the jth transversal mode can be directly deduced from the LO/TO splitting through the relation

$$\Delta\varepsilon_j = \frac{\varepsilon_\infty}{\omega_{jTO}^2}\frac{\prod_k(\omega_{kLO}^2-\omega_{kLO}^2)}{\prod_{k\neq j}(\omega_{kTO}^2-\omega_{jTO}^2)}. \tag{4}$$

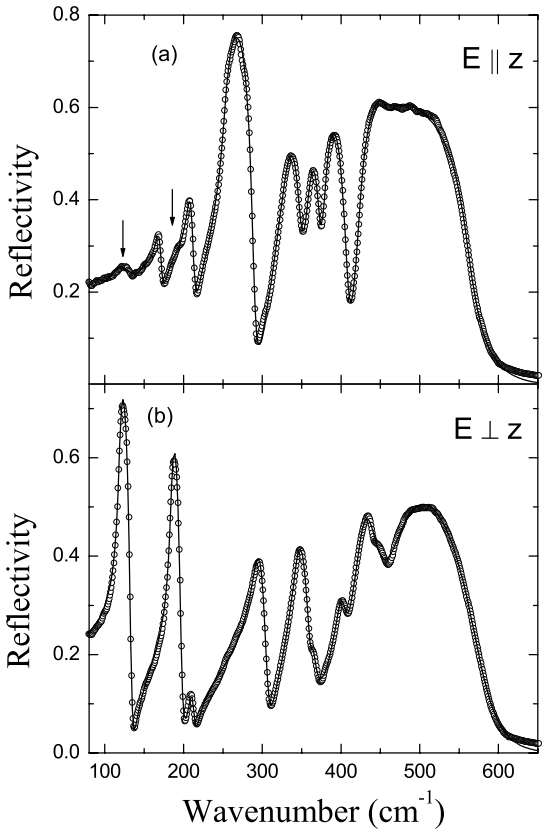

Figure 1. Infrared reflectivity of Li_2CaHfF_8 single crystals recorded with the electric field (a) parallel and (b) perpendicular to the z-axis. The open circles and full curve represent the experimental data and the best fit, respectively. Arrows indicate the bands associated with polarization leaks.

Values of the oscillator strength, calculated with equation (4), are presented in the fifth column of table 3. Thus, bands that leak in the $\boldsymbol{E} \parallel \boldsymbol{z}$ spectrum correspond to the strongest vibrational modes of the $\boldsymbol{E} \perp \boldsymbol{z}$ spectrum. Furthermore, the static dielectric constant can be obtained by adding the strength of all oscillators, that is

$$\varepsilon_0 = \varepsilon_\infty + \sum_j \Delta\varepsilon_j. \tag{5}$$

By using the previous equation we obtained the following values for the static dielectric constant: $\varepsilon_0^{\parallel} = 8.730$ and $\varepsilon_0^{\perp} = 7.148$ for radiation polarized parallel and perpendicular to the z-axis, respectively. These values agree very well with the results of impedance spectroscopy measurements reported by Ayala *et al* [8, 18]. These authors obtained, at 300 K and 100 kHz, values of 7.12 and 7.92 for the static dielectric constant parallel and perpendicular to the $\boldsymbol{z}$-axis, respectively. The proximity of these values to those obtained by infrared measurement results is due to the absence of polar domains and dipoles, the main contribution to the static dielectric constant arising from the polar phonons. At the other extreme of the infrared spectra, the values of the refraction index calculated from the high-frequency dielectric constant are approximately 1.5, which is in the range usually observed in fluoride crystals.

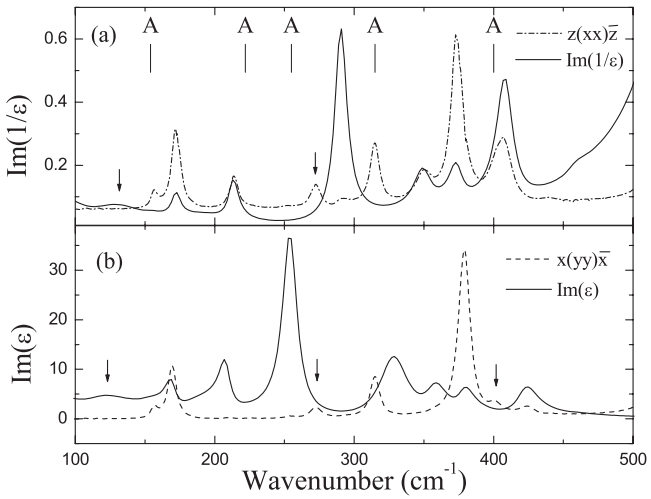

Figure 2. Optical function (ϵ'' and η'') derived from the four-parameter model fit of the Li_2CaHfF_8 reflectivity spectra in the $\boldsymbol{E} \parallel \boldsymbol{z}$ geometry. Raman spectra from [7] (in arbitrary units) are included for comparison. Arrows indicate the bands associated with oblique phonons and polarization leaks.

4. Discussion

In order to complete the analysis of the vibrational spectra of the Li_2CaHfF_8 scheelite, we will compare the phonons identified from the infrared reflectivity spectra with those obtained using Raman scattering. Ayala *et al* [7] used different scattering geometries to distinguish among the Raman-active irreducible representations. Thus, B(LO) modes are active in the $z(xy)\bar{z}$ configuration while B(LO) and A modes are mixed in the $z(xx)\bar{z}$ geometry. B(TO) modes are mixed with A modes in the $x(yy)\bar{x}$ geometry. Finally a mixture of E(TO) and E(LO) is observed in the $x(yz)\bar{x}$ scattering geometry.

The comparison between infrared and Raman results is best achieved by using the optical functions derived from the four-parameter semi-quantum model [16]. Thus, the frequencies of the maxima in the imaginary part of the complex dielectric constant (ε'') roughly correspond to the frequencies of transversal optical phonons. Furthermore, it is well known that the imaginary part of the reciprocal dielectric constant (η'') peaks at the frequencies of the longitudinal optical modes [19].

In figure 2, we plotted the optical function calculated from the fit of the $\boldsymbol{E} \parallel \boldsymbol{z}$ reflectivity spectrum compared with different Raman spectra. Since the intensities of the Raman and η'' peaks are originated in different physical processes, these magnitudes cannot be compared directly. This is not the case of the peak frequencies, which correspond to the same vibrational modes. In this way, figure 2(a) shows the η'' optical function (B(LO)) together with the $z(xx)\bar{z}$ Raman spectrum (A $\oplus$ B(LO)), while figure 2(b) shows the ε'' optical function (B(TO)) and the $x(yy)\bar{x}$ Raman spectrum (A $\oplus$ B(TO)). The frequency of the A modes is indicated to help in the discussion. The agreement between the results from the two techniques is remarkable, since for most of the peaks belonging to the B representation one peak in the optical functions is observed. However, some bands, indicated by arrows in figure 2, are only present in either Raman spectra or optical functions. This is the case of the low-wavenumber broad brand located around 120 cm^{-1} in both ϵ'' and η'' functions, which was previously associated with polarization leaks of E phonons in the reflectivity spectra. On the other hand, bands located

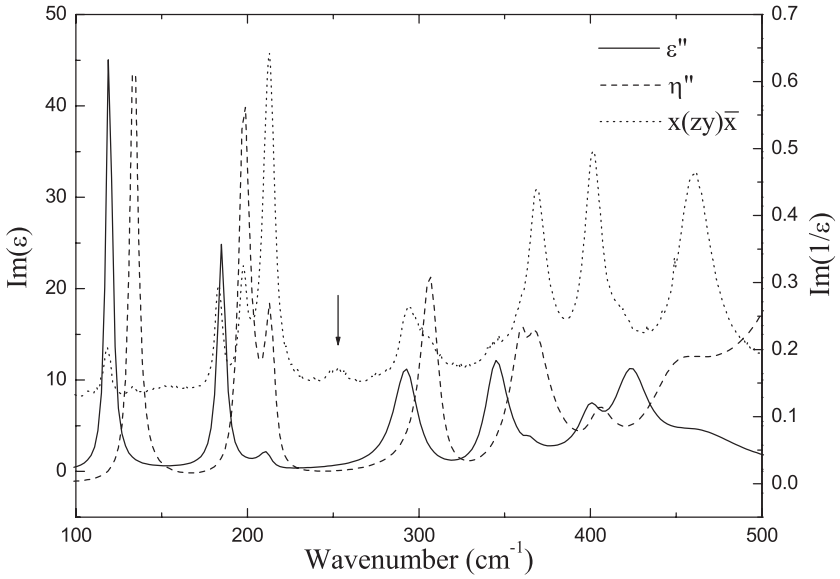

Figure 3. Optical function derived (ϵ'' and η'') from the four-parameter model fit of the Li_2CaHfF_8 reflectivity spectra in the $\boldsymbol{E} \perp \boldsymbol{z}$ geometry. Raman spectra from [7] (in arbitrary units) are included for comparison. The arrow indicates the band associated with oblique phonons.

at 273 and 403 cm^{-1} were reported by Ayala *et al* [7] in Raman spectra but they cannot be identified in the reflectivity measurement.

Following the comparison between the Raman and infrared studies, in figure 3 we show the ϵ'' and η'' optical functions calculated from the $\boldsymbol{E} \perp \boldsymbol{z}$ reflectivity spectrum together with the $x(zy)\bar{x}$ Raman spectrum. Notice that there is no scattering geometry that allows us to discriminate between the E(TO) and E(LO) modes in a Raman scattering experience. However, the fitting of the reflectivity spectrum using the four parameters of the semi-quantum model allows us to identify both components of the E irreducible representation. Thus, the comparison of the optical function with the Raman spectra shows an excellent agreement between them. As a consequence of this analysis, it is possible to observe that a band, located at 251 cm^{-1}, is only observed in the Raman spectrum and was erroneously associated with a E phonon [7].

The presence of the same bands in Raman spectra which are absent from infrared spectra can be understand by considering that the macroscopic electric field associated with polar modes modifies their frequencies. In the case of uniaxial crystals, if the wavevector $\hat{\boldsymbol{q}}$ is oriented parallel or perpendicular to the $\boldsymbol{c}$-axis, the modes can be classified as purely transverse or purely longitudinal depending on the orientation of the wavevector relative to the dipole carried by the phonon. In an arbitrary propagation direction, a strong dependence of the phonon frequency on the wavevector orientation should be observed. The normal mode frequency directional dispersion was widely discussed in [20–22] and is given by the roots of the equation

$$\left| (\omega_{iTO}^2 - \omega^2)\delta_{ij} + \frac{(\hat{\boldsymbol{q}} \cdot \boldsymbol{M}_i)(\hat{\boldsymbol{q}} \cdot \boldsymbol{M}_j)}{\varepsilon_\infty(\hat{\boldsymbol{q}})} \right| = 0, \tag{6}$$

with

$$\varepsilon_\infty(\hat{\boldsymbol{q}}) = \varepsilon_\infty^{\parallel} \cos^2\theta + \varepsilon_\infty^{\perp} \sin^2\theta. \tag{7}$$

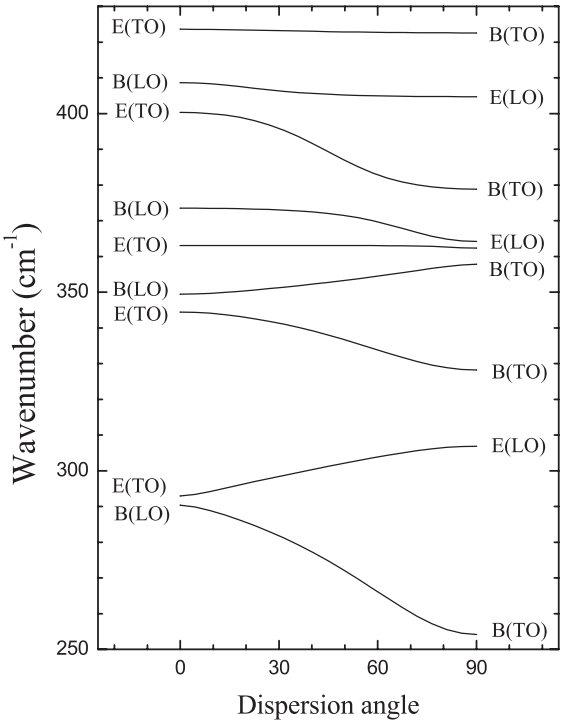

Figure 4. Angular dispersion of the Li_2CaHfF_8 polar modes between 250 and 430 cm^{-1}.

Here the normalized wavevector $\hat{\boldsymbol{q}}$ is inclined at an angle θ to the $\boldsymbol{c}$-axis. In our case, $\varepsilon_\infty^{\parallel}$ and $\varepsilon_\infty^{\perp}$ are given in table 3. $\boldsymbol{M_i}$ is the reduced dielectric polarization vector of the i-mode, which is simply related to the corresponding dielectric strength $\Delta\varepsilon_i$:

$$\Delta\varepsilon_i\omega_{iTO}^2 = |\boldsymbol{M_i}|^2. \tag{8}$$

Parameters listed in table 3 can be used to solve the equation (6) at different propagation angles. The calculated directional dispersion branches are shown in figure 4, where just the intermediate-frequency region (250–430 cm^{-1}) is plotted. Phonons which are decoupled from the others are called *ordinary*, and their frequencies are independent of the angle θ. The remaining phonons, which are coupled and show directional dispersion, are called *extraordinary* or *oblique*.

Based on the directional dispersion analysis, we are able to discuss the origin of the bands that were observed only in the Raman spectra. Thus, the band located at 273 cm^{-1} in figure 2 lies between the limits of the B(TO) (251 cm^{-1})–B(LO) (290 cm^{-1}) branch, which have a strong directional dispersion. Due to this fact, it should be originated in the propagation of an oblique mode. A similar conclusion can be achieved for the band at ∼403 cm^{-1}, which should be related to the branch B(TO) (350 cm^{-1})–E(TO) (401 cm^{-1}). This is an anomalous branch, since it does not connect transversal and longitudinal phonons. The existence of anomalous branches was explained by Loudon as arising from the competition of short- and long-range forces [23]. Oblique phonons belonging to these branches enable the propagation of mixed excitations with renormalized frequencies [20]. The band located at 251 cm^{-1} in figure 3 is at the same frequency as a B(TO) mode, and the branch to which it belongs has a strong angular dispersion. As a result, the weak B(TO) (251 cm^{-1}) phonon should be observed not

Table 4. Comparison of the energies (cm^{-1}) of the polar modes measured by infrared (IR) and Raman (R) spectroscopies.

A	B(TO)		B(LO)		E(TO)		E(LO)	
R	IR	R	IR	R	IR	R	IR	R
154	153	157	153	157	119	118	134	133
222	170	169	172	172	185	183	198	197
255	208	208	213	214	212	212	214	
315	254	253	290		293	293	307	304
400	329		349	350	344	345	362	358
532	358	357	374	374	363		364	
	379	378	409	408	400	401	405	
	423	423	458	439	424	417	445	
	458		561	532	465	461	578	585

as a polarization leak but as a oblique phonon in the $x(zy)\bar{x}$ spectrum. In consequence, bands observed only in Raman spectra could be associated with the propagation of oblique phonons, which should originate in either an orientation miss of the sample or the finite numeric aperture of the objective used in the microRaman equipment.

Finally, table 4 summarizes the classification of phonons observed by Raman and infrared spectroscopies. It is important to notice again the excellent agreement between the results of the two techniques. In this way, the complete vibrational spectrum of the Li_2CaHfF_8 scheelite is presented in this table.

5. Conclusion

High-precision single-crystal x-ray diffraction measurements of Li_2CaHfF_8 crystals confirm the proposed structure for this compound. According to our results, Li_2CaHfF_8 belongs to the $I\bar{4}$ space group with two molecules per unit cell and these atomic positions are listed in table 2. This structure is derived from the scheelite ones by taking out the inversion centre.

Once the crystalline structure was confirmed, polarized infrared reflectivity measurements were used to determine the transversal and longitudinal components of the polar phonons. By comparing these results with those previously reported from Raman spectra, we observe that the frequency of the phonons identified by each techniques agrees very well, but some bands are observed only in Raman spectra. The angular dispersion branches of polar modes were calculated and used to associate these bands with oblique phonons. As a result of these spectroscopic studies, the complete set of normal modes at the Brillouin zone centre was determined.

Acknowledgments

Financial support from CNPq, FUNCAP, FAPESP and the Millennium Institute: 'Water—a mineral approach' is gratefully acknowledged. The authors are grateful to Professor I Guedes for helpful discussions.

References

[1] Burkhalter R, Dohnke I and Hulliger J 2001 *Prog. Cryst. Growth Charact.* **42** 1
[2] Wyckoff R W G 1964 *Crystal Structures* vol 3, 2nd edn (New York: Interscience) p 19ff

[3] Garcia E and Ryan R R 1993 *Acta Crystallogr.* C **49** 2053
[4] *Landolt–Börnstein* 1973 *Numerical Data and Functional Relationship in Science and Technology* vol 7 (Berlin: Springer)
[5] Védrine A, Baraduc L and Cousseins J-C 1973 *MRS Bull.* **8** 581
[6] Védrine A, Trottier D, Cousseins J C and Chevalier R 1979 *MRS Bull.* **14** 583
[7] Ayala A P, Guedes I, Freire P T C, Sasaki J M, Mendes Filho J and Gesland J Y 1999 *J. Phys.: Condens. Matter* **11** 5343
[8] Ayala A P, Guedes I, Freire P T C, Sasaki J M, Mendes Filho J, Gesland J Y and Moreira R L 2000 *Solid State Ion.* **136/137** 345
[9] Enraf–Nonius 1997–2000 *COLLECT* (Delft: Nonius)
[10] Otwinowski Z and Minor W 1997 HKL Denzo and Scalepack *Methods in Enzymology* vol 276, ed C W Carter Jr and R M Sweet (New York: Academic) pp 307–26
[11] Blessing R H 1995 *Acta Crystallogr.* A **51** 33–8
[12] Sheldrick G M 1997 *SHELXS-97 Program for Crystal Structure Resolution* (Göttingen: University of Göttingen)
[13] Sheldrick G M 1997 *SHELXL-97 Program for Crystal Structures Analysis* (Göttingen: University of Göttingen)
[14] Farrugia L J 1997 ORTEP3 for Windows *J. Appl. Cryst.* **30** 565
[15] Rousseau D L, Bauman R P and Porto S P S 1981 *J. Raman Spectrosc.* **10** 253
[16] Gervais F and Pirou B 1974 *J. Phys. C: Solid State Phys.* **7** 2374
[17] Meneses D D 1999 *IRFit2.0 Adjustment Program* Orleans University (desouza@cnrs-orleans.fr)
[18] Ayala A P, Gesland J Y and Moreira R L 2001 private communication
[19] Gervais F 1983 High-temperature infrared reflectivity spectroscopy by scanning interferometry *Infrared and Millimetre Waves* vol 8, ed K J Button (New York: Academic) ch 7
[20] Shapiro S M and Axe J D 1972 *Phys. Rev.* B **6** 2420
[21] Claus R, Merten L and Brandmüller J 1975 *Light Scattering by Phonons Polaritons* (Berlin: Springer)
[22] Hayes W and Loudon R 1978 *Scattering of Light by Crystals* (New York: Wiley–Interscience)
[23] Loudon R 1969 *Light Scattering Spectra in Solids* ed C B Wright (New York: Springer)